

Photocatalytic Performances of ZnS/g-C₃N₄ Nanocomposites with Different Mass Ratios

Bilge Doğan¹, Agah Oktay Özdemir², Bülent Çağlar^{3*}, Eda Keleş Güner⁴

¹ Department of Chemistry, Institute of Science and Technology, Erzincan Binali Yıldırım University, Erzincan, Türkiye

² Department of Design, Vocational School, Erzincan Binali Yıldırım University, Erzincan, Türkiye

³ Department of Chemistry, Faculty of Arts and Sciences, Erzincan Binali Yıldırım University, Erzincan, Türkiye

⁴ Department of Property Protection and Security, Uzumlu Vocational School, Erzincan Binali Yıldırım University, 24150 Erzincan, Türkiye

Received: 25/05/2023, Revised: 07/07/2023, Accepted: 07/07/2023, Published: 28/03/2024

Abstract

In this study, we prepared a series of ZnS/graphitic-C₃N₄ nanocomposites in various mass percentages and morphological properties of all the nanocomposites were examined by utilizing SEM/EDX technique. The photocatalytic performances of ZnS/graphitic-C₃N₄ nanocomposites were evaluated by degradation of Rhodamine B molecules under visible light. The photocatalytic performances of all nanocomposites under various photocatalyst dosages and initial Rhodamine B concentrations were further investigated for determination of optimal conditions. The obtained results indicated that ZnS/graphitic-C₃N₄ nanocomposites show almost 2 times higher photocatalytic performances than pure graphitic-C₃N₄ and ZnS nanoparticles. The scavenger studies indicated that the superoxide radicals had a major role in the photodegradation and the photodegradation of Rhodamine B follows the pseudo-first-order kinetic.

Keywords: g-C₃N₄, mechanism, photocatalysis, ZnS nanoparticles

Farklı Kütle Oranlarına Sahip ZnS/g-C₃N₄ Nanokompozitlerin Fotokatalitik Performansları

Öz

Bu çalışmada, çeşitli kütle yüzdelerinde bir seri ZnS/grafit-C₃N₄ nanokompozitler hazırladık ve bütün bu nanokompozitlerin morfolojik özellikleri SEM/EDX tekniği kullanılarak incelendi. ZnS/grafitik-C₃N₄ nanokompozitlerinin fotokatalitik performansları, Rhodamine B moleküllerinin görünür ışık altında parçalanmasıyla değerlendirildi. Optimum koşulların belirlenmesi için tüm nanokompozitlerin fotokatalitik performansları çeşitli fotokatalizör miktarları ve başlangıç Rhodamine B derişimleri için incelendi. Elde edilen sonuçlar, ZnS/grafitik-C₃N₄ nanokompozitlerin saf grafitik-C₃N₄ ve ZnS nanoparçacıklarına nispeten yaklaşık 2 kat daha yüksek fotokatalitik performans gösterdiğini ortaya koymuştur. Süpürücü çalışmaları, süperoksit radikallerinin fotobozunmada önemli bir role sahip olduğunu ve Rhodamine B'nin fotobozunmasının yalancı birinci dereceden kinetiği takip ettiğini göstermiştir.

Anahtar Kelimeler: g-C₃N₄, mekanizma, fotokataliz, ZnS nanoparçacıklar

*Corresponding Author: bcaglar@erzincan.edu.tr

Bilge DOĞAN, <https://orcid.org/0000-0001-7552-3461>

Agah Oktay ÖZDEMİR, <https://orcid.org/0000-0003-4488-746X>

Bülent ÇAĞLAR, <https://orcid.org/0000-0002-6087-3685>

Eda KELEŞ GÜNER, <https://orcid.org/0000-0002-4421-1315>

1. Introduction

Increase in the utilization of hazardous dyes in industrial areas such as rubber, plastic, textile, paint, printing, pharmaceutical, leather have caused the accumulation of these toxic dye molecules in water resources, effecting aquatic life, human health and ecosystem [1-3]. Therefore, improving some influential techniques for removal of these pollutants in wastewater is important sense to the ecosystem, aquatic life and human health [4-5]. Hence, various biological, physical and chemical techniques such as filtration, adsorption, precipitation, chemical reduction and oxidation, flocculation, microbial treatment and photocatalysis have used to the wastewater purifications [6-10]. Among them, photocatalysis has been widely used for the degradation of permanent dye pollutants from wastewater due to its effectively, high performance rate, simplicity, operational simplicity, low cost, stability, good reusibility as well as being green technology [11]. To degrade dye pollutants from wastewater, reactive oxygen species like hole-electron pairs, hydroxyl and superoxide radicals are produced by irradiation of photocatalysts in photocatalysis [12]. Thereafter, generated these species degrade pollutants into nontoxic products as well as carbon dioxide, water and oxygen molecules [13]. Diverse photocatalysts such as ZnO, TiO₂, CuO and CdS semiconductors have been extensively conducted for degradation of dye molecules in [14-17]. However, these mentioned photocatalysts can be used in existence of UV irradiation because of wide band gap values, which restricted their practical photocatalysis processes under presence of visible light. Therefore, numerous research groups have improved new photocatalytic materials for the influential utilization in photocatalysis under visible light [4,5,12,13]. Among these photocatalytic materials, graphitic carbon nitride (g-C₃N₄) has been widely attracted for the degradation of dye pollutants because of narrow band gap value, low cost, thermal stability and ability to absorb visible light [18-20]. Nevertheless, the fast electron-hole pairs recombination property of g-C₃N₄ limits photocatalytic activity [18-20]. To prevent the electron-hole pairs recombination and develop the photocatalytic performance of g-C₃N₄, coupling with proper semiconductor materials to produce heterostructure materials and nanocomposites [18-20].

In the present study, we synthesized ZnS/g-C₃N₄ nanocomposites at different mass ratios and morphological properties of these nanocomposites were examined by SEM/EDX technique. The photocatalytic performances of the synthesized nanocomposites were investigated for degradation of RhB under visible light irradiation. The effects of initial RhB concentration and photocatalysts dosages and kinetic of photodegradation were also examined for the definition of optimal conditions. The mechanism of photocatalysis process was proposed by using various scavengers such as tert-butyl alcohol (TBA), L-ascorbic acid (LA), ethylenediaminetetraacetic acid disodium salt (EDTA) and AgNO₃.

2. Material and Methods

2.1. Materials

Zinc nitrate hexahydrate (Zn(NO₃)₂·6H₂O), melamine, thioacetamide, ethylene glycol, 2,6-Di-tert-butyl-4-methylphenol bic acid, ethylenediaminetetraacetic acid disodium salt and AgNO₃ were purchased from Sigma-Aldrich.

2.2. Synthesis of ZnS Nanoparticles

0.004 mol Zn(NO₃)₂·6H₂O and 0.012 mol thioacetamide were separately dissolved in ethylene glycol (30 mL). Then dissolved thioacetamide solution was slowly added dropwise into the dissolved Zn(NO₃)₂·6H₂O solution and stirring for 1 hour at room temperature. Then, the obtained homogeneous solution was transferred to a Teflon-coated stainless steel autoclave. The autoclave heated up 170 °C and it was kept at 170 °C for 14 hours and then naturally cooled to room temperature. The obtained solid product was filtered and washed with distilled water and ethanol three times. Then solid sample was dried at 80 °C for 12 hours and obtained an off-white powder (ZnS nanoparticles).

2.3. Synthesis of g-C₃N₄

The muffle furnace was purged with Ar gas for 10 min and then the heating rate is programmed to increase from 25 °C to 580 °C in 3 hours, to wait at 580 °C for 30 minutes and to cool in 30 minutes. After, 5 g melamine was placed in a crucible and melamine was annealed under these programmed conditions in the muffle furnace and obtained yellow powder (g-C₃N₄) was grinded in a mortar.

2.4. Synthesis of ZnS/g-C₃N₄ Nanocomposites

0.004 mol Zn(NO₃)₂·6H₂O was dissolved in ethylene glycol (25 mL). 390 mg of g-C₃N₄ was well dispersed in ethylene glycol (10 mL) in other beaker. The g-C₃N₄ dispersion was added into the dissolved Zn(NO₃)₂·6H₂O solution and mixture was stirred under these conditions for 30 min. Then, dissolved thioacetamide in ethylene glycol (25 mL) was slowly added dropwise to the prepared mixture. After the addition was completed, the mixture was stirred at room temperature at high speed for 1 hour. The mixture was transferred to a Teflon coated stainless steel autoclave and it was kept in an autoclave at 170 °C for 14 hours and then rapidly cooled to room temperature. The obtained solid powder was filtered and washed with distilled water and ethanol three times separately. The solid sample was dried at 80 °C for 12 hours and the ZnS/g-C₃N₄ nanocomposite was obtained in a 1:1 ratio and labelled as ZnS/g-C₃N₄ 1:1. ZnS/g-C₃N₄ 2:1 and ZnS/g-C₃N₄ 1:2 nanocomposites were synthesized by using a similar synthesis method.

2.5. Measurement of Photocatalytic Activities of Samples

The studies of photocatalytic activities of g-C₃N₄, ZnS, ZnS/g-C₃N₄ 1:2, ZnS/g-C₃N₄ 1:1 and ZnS/g-C₃N₄ 2:1 samples were examined via photodegradation of RhB dyestuff under visible light in photoreactor (Luzchem, LZC-4X). The photocatalysts (2g/L) and dyestuff solution (5mg/L) were stirred without irradiation (in the dark) for 60 min to attain the adsorption/desorption equilibrium between dyestuff molecules and photocatalysts. After the adsorption/desorption equilibrium, 2mL was taken from suspension, centrifuged and measured the absorbance value at 554nm for determination of initial concentration (C₀) of RhB dyestuff. Then, the mixtures were exposed to visible-light irradiation for an extended irradiation time under

stirring. At determined time intervals, 2mL suspensions was extrated and centrifuged to remove the solid photocatalysts. Then dye concentration (C_t) at given time in centrifuged solution was determined via measuring the absorbance value at maximum wavelength (554nm) by utilizing UV-vis spectrometer. Finally, the photodegradation activities were calculated according to Eq.(1) given below.

$$\text{Photodegradation (\%)} = \frac{C_0 - C_t}{C_0} \times 100 \quad (1)$$

The influence of catalyst dosage (1-3g/L) and initial RhB dye concentration (5-15mg/L) on photodegradation activities of photocatalysts were examined under same experimental procedure at determined pH value.

2.6. Instruments

The SEM-EDX analysis to obtained morphological features and elemental composition of samples were taken on a Field Emission Scanning Electron Microscope (Quanta FEG 450-FEI). PG Instrument T80+ model UV-Vis spectrophotometer was used in photocatalytic activity studies of samples.

3. Results and Discussion

3.1. SEM-EDX analysis of samples

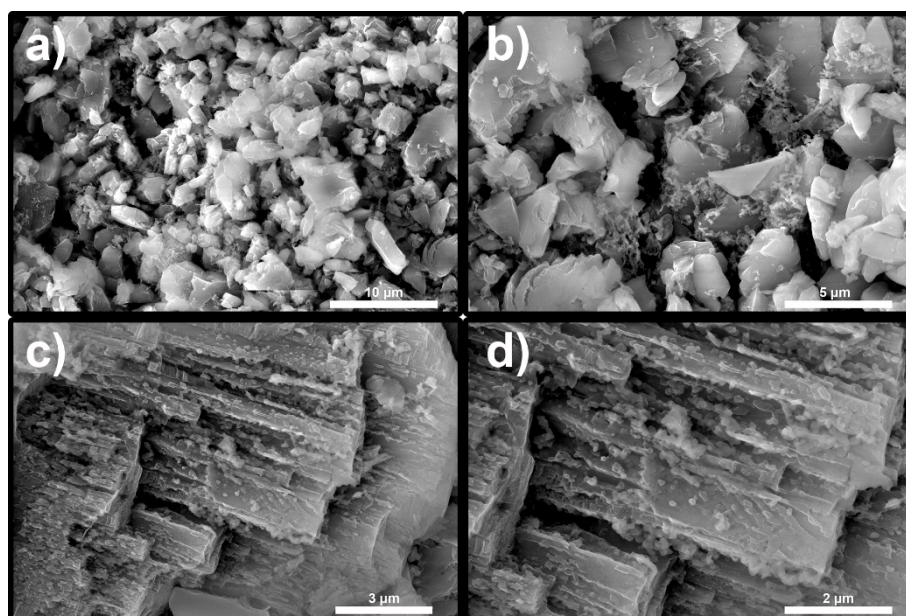


Figure 1. SEM images of g-C₃N₄ at different magnifications

The morphological features of g-C₃N₄, ZnS, ZnS/g-C₃N₄ 1:2, ZnS/g-C₃N₄ 1:1 and ZnS/g-C₃N₄ 2:1 samples were investigated by SEM analysis. As illustrated as **Fig. 1a-d**, pure g-C₃N₄ showed a layered stacking morphology with roughness surface which provide an advantage for

decoration of ZnS nanoparticles on its surface. ZnS have mostly exhibited the nano-sphere structure together with considerable aggregation (**Fig. 2a-d**). The SEM images of ZnS/g-C₃N₄ 1:2, ZnS/g-C₃N₄ 1:1 and ZnS/g-C₃N₄ 2:1 nanocomposites evidently showed that ZnS nano-spheres covered on g-C₃N₄ sheets with well dispersion, which supplied direct proof for the successful synthesis of ZnS/g-C₃N₄ nanocomposites (**Fig. 3-5 a-d**). As it is known, the decrease in aggregation of ZnS nanoparticles on g-C₃N₄ sheets increases the photocatalytic performances of nanocomposites via providing more active sites [21]. However, the appropriate quantity ratios of materials are also significant parameter to improve the photocatalytic performances of nanocomposites [18-21]. The SEM images of ZnS/g-C₃N₄ nanocomposites demonstrated that the aggregation of ZnS nano-spheres on g-C₃N₄ surface decreased with the amount of ZnS loaded.

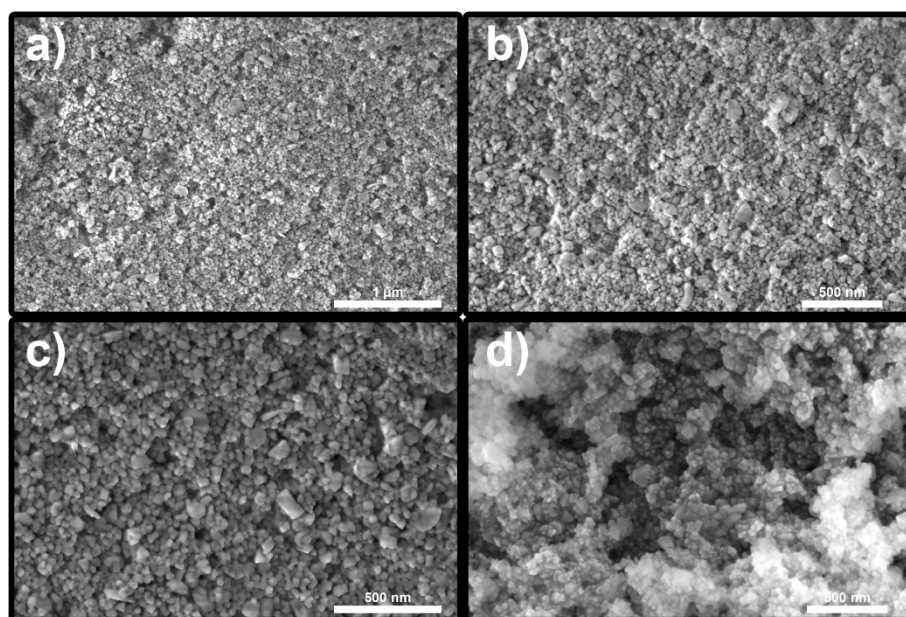


Figure 2. SEM images of ZnS nanoparticles at different magnifications

The elemental composition of g-C₃N₄, ZnS, ZnS/g-C₃N₄ 1:2, ZnS/g-C₃N₄ 1:1 and g- ZnS/g-C₃N₄ 2:1 samples were performed by using EDX analysis and EDX spectra of samples were given in (**Fig. 6**). The atomic % of elements on the samples were also given in the inset of (**Fig. 6**). The pure g-C₃N₄ have only C and N atoms while pure ZnS contains Zn and S atoms, which are in well agreement with stoichiometric ratio of their formula's components. The EDX data of ZnS/g-C₃N₄ nanocomposites indicate the existence of C, N, Zn and S elements which confirmed the successful formation of ZnS/g-C₃N₄ nanocomposites with good purities. The tight connection between ZnS and g-C₃N₄ provides prevention of recombination of holes and electrons, which increases the catalytic activities of nanocomposites [21].

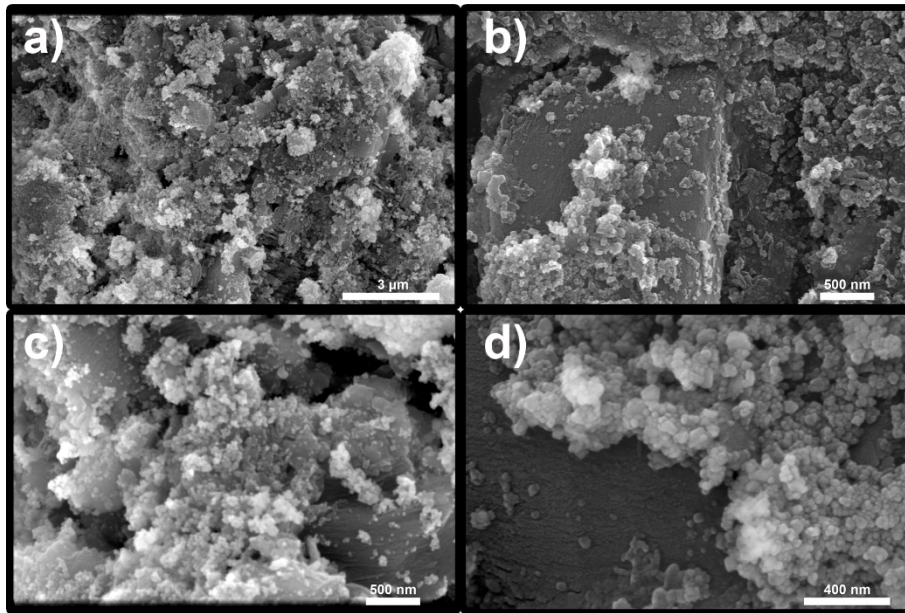


Figure 3. SEM images of ZnS/g-C₃N₄ 1:2 nanocomposite at different magnifications

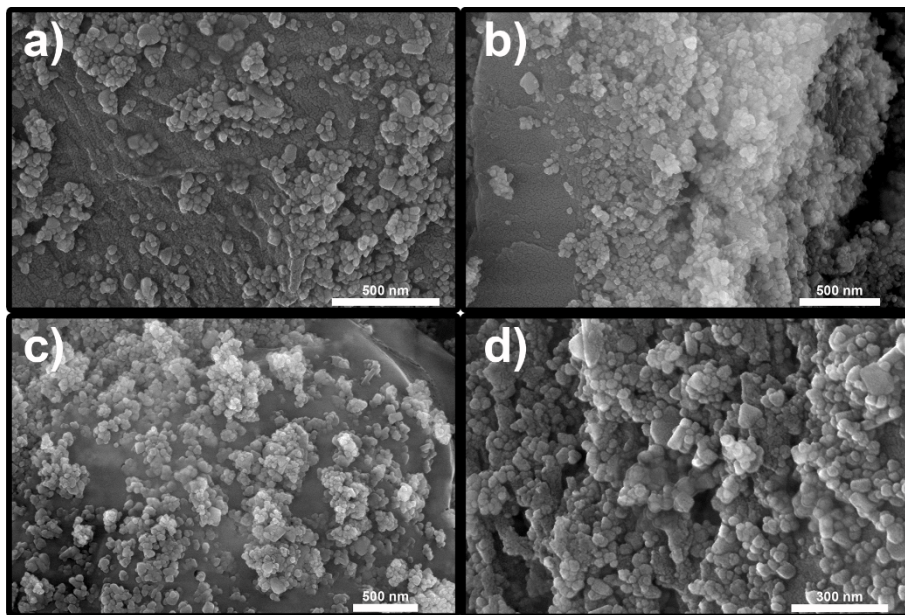


Figure 4. SEM images of ZnS/g-C₃N₄ 1:1 nanocomposite at different magnifications

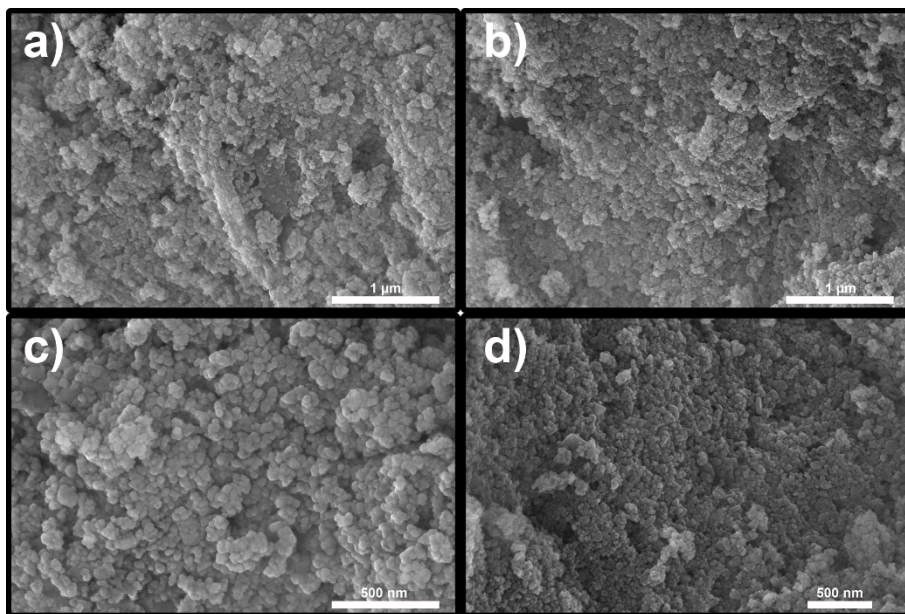


Figure 5. SEM images of ZnS/g-C₃N₄ 2:1 nanocomposite at different magnifications

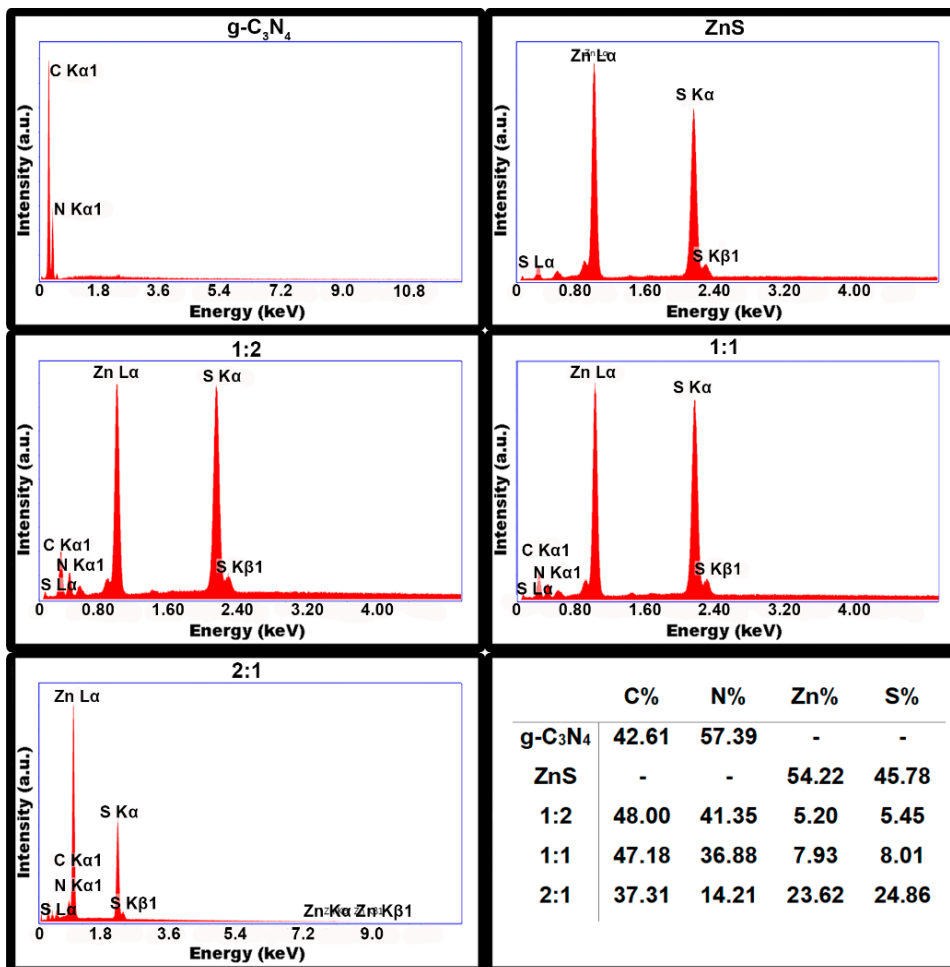


Figure 6. EDX spectra and atomic mass ratio of samples

3.2. Photocatalytic degradation of Rhodamine B

The photocatalyst dosage, initial solution pH and initial dye concentration are important parameters affecting photocatalytic activity in addition to the surface area, particle size and aggregation of the photocatalyst. Therefore, the effect of catalyst dosage and initial dye concentration on the photodegradation of RhB dyestuff under visible light were investigated in the presence of ZnS/g-C₃N₄ 1:2, ZnS/g-C₃N₄ 1:1 and ZnS/g-C₃N₄ 2:1 catalyst. In order to examine the effect of the photocatalyst dosage on the photodegradation of RhB, the photocatalyst dosages were taken as 1, 2 and 3 g/L at pH 6,36 for an initial dyestuff concentration of 5 mg/L. When the catalyst dosages are taken as 1, 2 and 3 g/L, the photodegradation of RhB molecules were determined as 87%, 92% and 95% for the ZnS/g-C₃N₄ 1:2 catalysts, 68%, 92% and 91% for ZnS/g-C₃N₄ 1:1 catalyst, and also 68%, 79% and 75% for ZnS/g-C₃N₄ 2:1 catalyst, respectively (**Fig.7a-c**). It was found that the photodegradation efficiencies of all catalysts towards RhB increased when catalyst dosage was increased from 1g/L to 2g/L whereas the photodegradation efficiencies decreased after the catalyst dosage was increased to 3g/L. The increases in photodegradation efficiencies is associated with an increase in the amount of active centers on the catalyst surface responsible for the adsorption of dye molecules, depending on the amount of catalyst [12,13,22]. On the other hand, while an increase in the photodegradation of RhB was expected due to the increase in the catalyst dosage, but it was found to a decrease [22]. This situation is explained by the scattering of light by suspension due to the increase in the opacity of the suspension with the increasing amount of catalyst and thus preventing the light from reaching the active centers on the catalyst surface [12,13,22]. According to the catalyst dosage studies, the best catalyst dosage was determined as 2g/L for all catalysts.

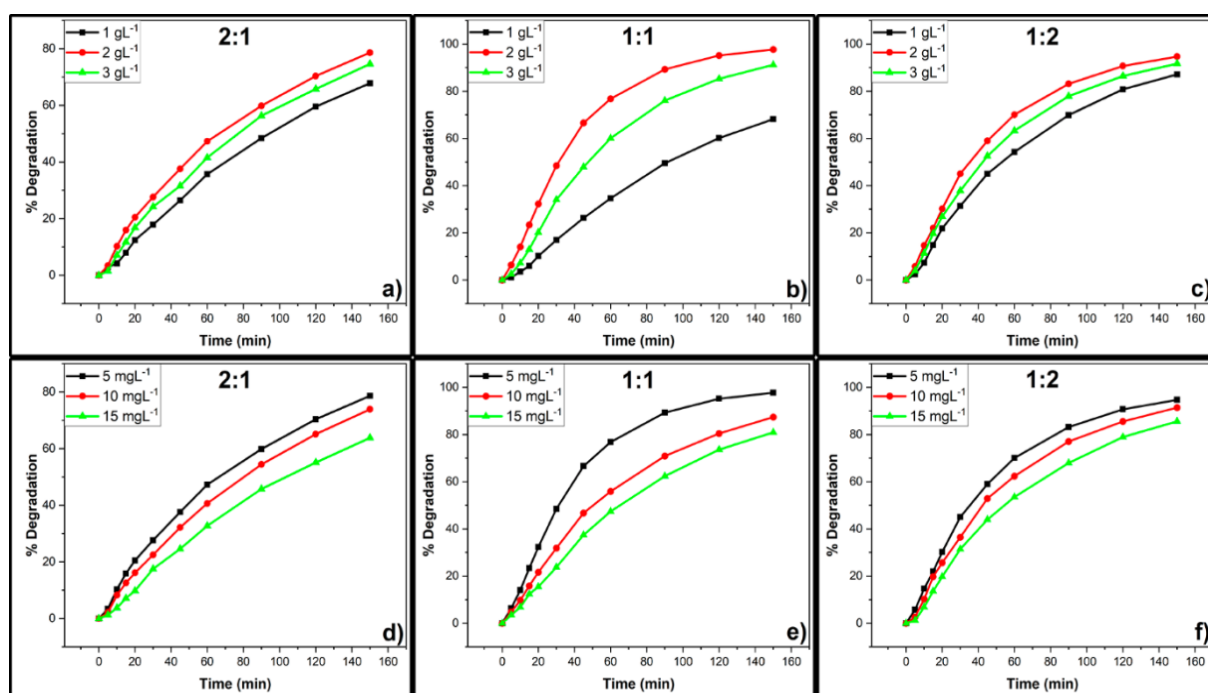


Figure 7. The influence of the photocatalyst dosage (a,b,c) and initial dye concentration (d,e,f) on the photodegradation of RhB

To investigate the influence of the initial dye concentration on the photodegradation of RhB, the initial dye concentrations were taken as 5, 10 and 15 mg/L at pH 6.36 using 2g/L catalyst dosage. When the initial dye concentrations were taken as 5, 10 and 15 mg/L, the photodegradation of RhB molecules were detected as 95%, 91% and 85% for the ZnS/g-C₃N₄ 1:2 catalysts, 98%, 87% and 81% for ZnS/g-C₃N₄ 1:1 catalyst, and also 79%, 74% and 64% for ZnS/g-C₃N₄ 2:1 catalyst, respectively (**Fig. 7d-f**). As seen from Fig. 7d-f, it was observed that the photodegradation efficiencies of all catalysts were decreased by increasing the initial dye concentration. This situation is associated with the fact that increasing dye concentration causes an increase in the amount of non-adsorbed dye molecules [12,13,23]. These non-adsorbed dye molecules cause both a decrease in the light transmittance and a prevent the penetration of the light used on the catalyst surface due to the characteristic light absorption ability of the dye molecules [12,13,23]. These events induce a decrease in the amount of photodegradation. According to the initial dye concentration studies, the most appropriate initial dye amount was found as 5mg/L.

We further investigated the photocatalytic activities of pure g-C₃N₄, pure ZnS and ZnS/g-C₃N₄ nanocomposites by examining photodegradation of RhB molecules under visible light in the determined optimum conditions (5mg/L initial dye concentration, 1g/L catalyst dosage, and pH=6.36) and the obtained results are showed in (**Fig. 8a**). Photolysis of RhB was detected as 10 % under visible light within 150 minutes without the presence of any catalyst. In the presence of ZnS and g-C₃N₄ catalysts, the photodegradation of RhB under the same conditions was found to be 43% and 70%, respectively. The photocatalytic performances of ZnS/g-C₃N₄ heterostructures significantly increased compared to pure g-C₃N₄ and ZnS. The photocatalytic performances of ZnS/g-C₃N₄ 1:2; ZnS/g-C₃N₄ 1:1 and ZnS/g-C₃N₄ 2:1 photocatalysts were detected as 95%, 98% and 79%, respectively, which showed that ZnS/g-C₃N₄ heterostructures have satisfactory photocatalytic performances. The production of heterojunction structure between the g-C₃N₄ and ZnS facilitated the electron transition from g-C₃N₄ to ZnS and thus resulted in preventing of the recombination of hole-electron pairs, which increases the photocatalytic performance of nanocomposites. The ZnS/g-C₃N₄ 1:1 nanocomposite indicated the best photocatalytic performance which degraded 98 % of RhB molecules after visible light irradiation for 150 minutes.

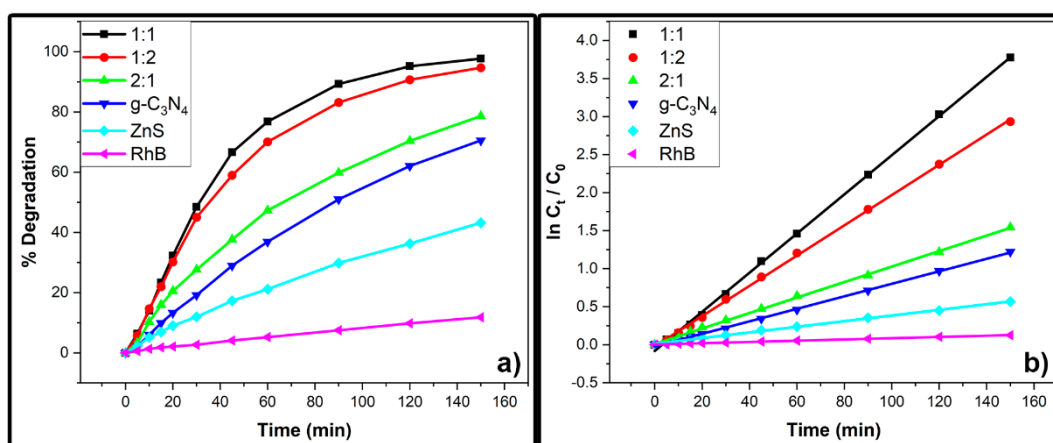


Figure 8. The photocatalytic performances of samples under optimum conditions

To determine the kinetic parameters, the pseudo-first-order kinetic model was performed according to equation is given below. **Fig. 8b** showed that a plot of $\ln(C_0/C_t)$ versus time have straight lines for all samples, proving degradation reaction of RhB in the presence of all samples follow the pseudo-first-order kinetic.

$$\ln \frac{C_0}{C_t} = k_{app} \cdot t \quad (2)$$

The C_0 , C_t and t are the initial concentration of dye molecules, the concentration of dye molecules at the relevant irradiation time and time (minute), respectively. The k_{app} is the apparent rate constant (min^{-1}) which obtained from the slope of the plot of $\ln(C_0/C_t)$ versus time. In addition, the calculated k_{app} constants and correlation coefficients (R^2) values are offered in **Table 1**. The k_{app} and R^2 values of ZnS/g-C₃N₄ 1:1 nanocomposite are highly higher than those of g-C₃N₄, ZnS and other ZnS/g-C₃N₄ nanocomposites. Therefore, these data showed that the photodegradation of RhB in the existence of ZnS/g-C₃N₄ 1:1 nanocomposite fits the pseudo-first-order kinetic very well and it has the supreme photocatalytic performance.

Table 1. The calculated k_{app} constants and correlation coefficients (R^2)

Samples	k_{app} (dak^{-1})	R^2
g-C ₃ N ₄	0.00822	0.99944
ZnS	0.00371	0.99844
1:1	0.02574	0.99925
1:2	0.01685	0.99961
2:1	0.01018	0.99920

In order to find the influences of reactive species to photodegradation of RhB on ZnS/g-C₃N₄ catalyts and to evaluate the catalytic mechanism, the trapping studies were carried out the same experimental conditions as photocatalysis studies. Tert-butyl alcohol (TBA), L-ascorbic acid (LA), ethylenediaminetetraacetic acid disodium salt (EDTA) and AgNO₃ were utilized as the scavengers to evaluate the effect of hydroxyls radicals, superoxide radicals, holes and electrons, respectively. **Fig. 9** shows the photocatalytic performances of ZnS/g-C₃N₄ catalyts for the RhB photodegradation under visible light the existence of the scavengers and except of the addition of them. The scavenger results indicate that the roles of scavengers in the order of superoxide radicals > holes > electrons and hydroxyls radicals. The superoxide radicals and holes have primary and secondary roles in the photodegradation of RhB, respectively, whereas electrons and hydroxyls radicals have minor roles in the photodegradation of RhB.

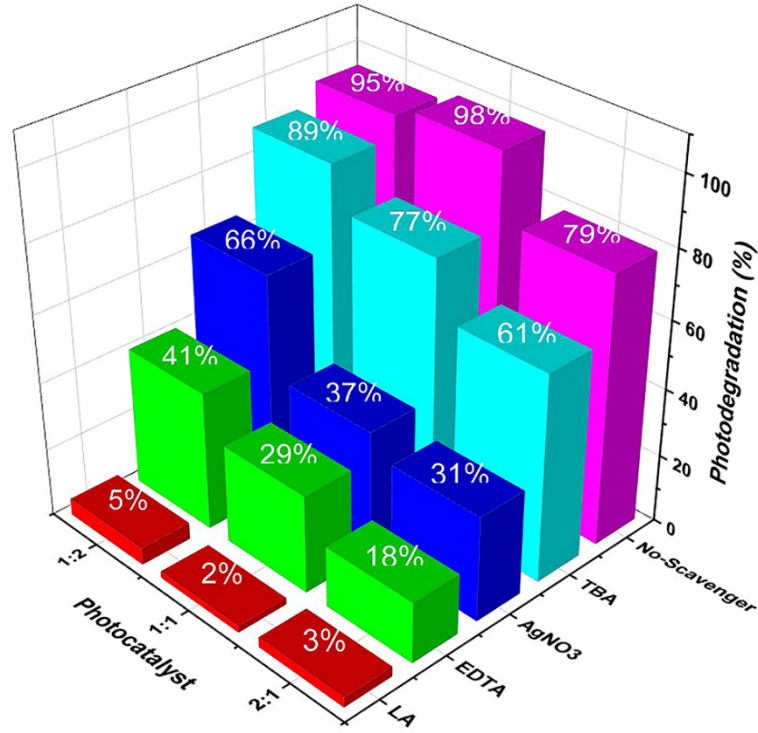


Figure 9. The effects of scavengers on the photodegradation of RhB

According to the literature, the band gap values of g-C₃N₄ and ZnS are approximately 2.5 and 3.9 eV. [19]. Therefore, the g-C₃N₄ can be photoexcited by visible light whereas ZnS cannot be photoexcited by visible light. Based on the band gap values and scavenger studies, the plausible mechanism for degradation of RhB under visible light in presence of all ZnS/g-C₃N₄ catalyts was given in following equations [3-7].



4. Conclusion

ZnS/g-C₃N₄ nanocomposites with various mass percentages were synthesized and characterized by SEM/EDX analysis. The ZnS/g-C₃N₄ 1:1 nanocomposite showed excellent visible-light-driven photocatalytic performance. The obtained results indicated that the photocatalytic performances of the synthesized materials against RhB molecules in order of ZnS/g-C₃N₄ 1:1, ZnS/g-C₃N₄ 1:2, ZnS/g-C₃N₄ 2:1, g-C₃N₄ and ZnS. The superoxide radicals have principle roles while other species play minor effects in the photodegradation of RhB. The degradation of RhB molecules existence of all photocatalysts was determined to follow the pseudo-first-order kinetic. This present work provides novel approach for improving ZnS/g-C₃N₄ nanocomposites for photodegradation of various pollutants.

Ethics in Publishing

There are no ethical issues regarding the publication of this study.

Author Contributions

All authors contributed equally to the writing of this manuscript

Acknowledgements

This study was produced from Bilge Doğan's PhD thesis. Bilge Doğan was supported by YÖK as a 100/2000 scholar in the priority field (micro and nanotechnology) during her PhD thesis.

References

- [1] Ren, Z., Zhu, B., Xia, J., Ming, M., Zhang, S., Zhi, X., Chen, S., Zhang, W., (2023) High quality factor infrared notch filter with compact electromagnetically induced transparency metamaterial structure, *Materials Letters*, 343, 134349.
- [2] Wang, P., Zhong, S., Lin, M., Lin, C., Lin, T., Gao, M., Zhao, C., Li, X., Wu, X., (2022) Signally enhanced piezo-photocatalysis of Bi_{0.5}Na_{0.5}TiO₃/MWCNTs composite for degradation of rhodamine B, *Chemosphere*, 308, 136596.
- [3] Xu, D., Ma, H., (2021) Degradation of rhodamine B in water by ultrasound-assisted TiO₂ photocatalysis, *Journal of Cleaner Production*, 313, 127758.
- [4] Kong, H., Li, H., Wang, H., Li, S., Lu, B., Zhao, J., Cai, Q., (2023) Fe-Mo-O doping g-C₃N₄ exfoliated composite for removal of rhodamine B by advanced oxidation and photocatalysis, *Applied Surface Science*, 610, 155544.
- [5] Ashok, B., Ramesh, K., Madhu, D., Nagesh, T., Vijaya Kumar, B., Upender, G., (2023) Characterization and photocatalysis of visible light driven Z-scheme Bi₂WO₆/Bi₂MoO₆

heterojunction for Rhodamine B degradation, *Inorganic Chemistry Communications*, 150, 110495.

[6] Mittal, H., Al Alili, A., Morajkar, P. P., Alhassan, S. M., (2021) Graphene oxide crosslinked hydrogel nanocomposites of xanthan gum for the adsorption of crystal violet dye, *Journal of Molecular Liquids*, 323, 115034.

[7] Khumalo, N. P., Nthunya, L. N., De Canck, E., Derese, S., Verliefdde, A. R., Kuvarega, A. T., Mamba, B. B., Mhlanga, S. D. Dlamini, D. S., (2019) Congo red dye removal by direct membrane distillation using PVDF/PTFE membrane, *Separation and Purification Technology*, 211, 578- 586.

[8] Menon, P., Anantha Singh, T. S., Pani, N., Nidheesh, P. V., (2021) Electro-Fenton assisted sonication for removal of ammoniacal nitrogen and organic matter from dye intermediate industrial wastewater, *Chemosphere*, 269, 128739.

[9] Tekin, D., Tekin, T., Kiziltas, H., (2020) Synthesis and characterization of TiO₂ and Ag/TiO₂ thin-film photocatalysts and their efficiency in the photocatalytic degradation kinetics of Orange G dyestuff, 198, 376- 385.

[10] Giwa, A., Yusuf, A., Balogun, H. A., Sambudi, N. S., Bilad, M. R., Adeyemi, I., Chakraborty, S., Curcio, S., (2021) Recent advances in advanced oxidation processes for removal of contaminants from water: A comprehensive review, *Process Safety and Environmental Protection*, 146, 220- 256.

[11] Pera-Titus, M., García-Molina, V., Baños, M. A., Giménez, J., Esplugas, S., (2004) Degradation of chlorophenols by means of advanced oxidation processes: a general review, *Applied Catalysis B: Environmental*, 47(4), 219- 256.

[12] Caglar, B., Keles Guner, E., Ersoy, S., Caglar, S., Özdemir, A. O., Özdokur, K. V., Doğan, B., İçer, F., Çırak, Ç., (2021) Bi₂S₃ nanorods decorated on bentonite nanocomposite for enhanced visible-light-driven photocatalytic performance towards degradation of organic dyes, *Journal of Alloys and Compounds*, 885, 160964.

[13] Caglar, B., Keles Guner, E., Özdokur, K. V., Özdemir, A. O. İçer, F., Caglar, S., Doğan, B., Beşer, B. M. Çırak, Ç., Tabak, A., Ersoy, S., (2021) Application of BiFeO₃ and Au/BiFeO₃ decorated kaolinite nanocomposites as efficient photocatalyst for degradation of dye and electrocatalyst for oxygen reduction reaction, *Journal of Photochemistry and Photobiology A: Chemistry*, 418, 113400.

[14] Chen, X., Wu, Z., Liu, D., Gao, Z., (2017) Preparation of ZnO Photocatalyst for the Efficient and Rapid Photocatalytic Degradation of Azo Dyes, *Nanoscale Research Letters*, 12(1), 1-10.

[15] Tao, C., Jia, Q., Han, B., Ma, Z., (2020) Tunable selectivity of radical generation over TiO₂ for photocatalysis, *Chemical Engineering Science*, 214, 115438.

- [16] Sahu, K., Choudhary, S., Khan, S. A., Pandey, A., Mohapatra, S., (2019) Thermal evolution of morphological, structural, optical and photocatalytic properties of CuO thin films, *Nano-Structures & Nano-Objects*, 17, 92- 102.
- [17] Dey, P. C., Das, R., (2020) Enhanced photocatalytic degradation of methyl orange dye on interaction with synthesized ligand free CdS nanocrystals under visible light illumination, *Spectrochimica Acta Part A: Molecular and Biomolecular Spectroscopy*, 231, 118122.
- [18] Ma, Y., Li, J., Cai, J., Zhong, L., Lang, Y., Ma, Q., (2022) Z-scheme g-C₃N₄/ZnS heterojunction photocatalyst: One-pot synthesis, interfacial structure regulation, and improved photocatalysis activity for bisphenol A, *Colloids and Surfaces A: Physicochemical and Engineering Aspects*, 653, 130027.
- [19] Palanisamy, G., Al-Shaalan, N. H., Bhuvaneswari, K., Bharathi, G., Bharath, G., Pazhanivel, T., Sathishkumar, V. E., Arumugam, M. K., Pasha, S. K. K., Habila, M. A., El-Marghany, A., (2021) An efficient and magnetically recoverable g-C₃N₄/ZnS/CoFe₂O₄ nanocomposite for sustainable photodegradation of organic dye under UV-visible light illumination, *Environmental Research*, 201, 111429.
- [20] Danish, M., Muneer, M., (2021) Excellent visible-light-driven Ni-ZnS/g-C₃N₄ photocatalyst for enhanced pollutants degradation performance: Insight into the photocatalytic mechanism and adsorption isotherm, *Applied Surface Science*, 563, 150262.
- [21] Yan, Y., Yang, M., Wang, C., Liu, E., Hu, X., Fan, J., (2019) Defected ZnS/bulk g-C₃N₄ heterojunction with enhanced photocatalytic activity for dyes oxidation and Cr (VI) reduction, *Colloids and Surfaces A: Physicochemical and Engineering Aspects*, 582, 123861.
- [22] Liu, Y., Ding, S., Xu, J., Zhang, H., Yang, S., Duan, X., Sun, H., Wang, S., (2017) Preparation of a p-n heterojunction BiFeO₃@TiO₂ photocatalyst with a core-shell structure for visible-light photocatalytic degradation, *Chinese Journal of Catalysis*, 38(6), 1052- 1062.
- [23] Chakrabarti, S., Dutta, B. K., (2004) Photocatalytic degradation of model textile dyes in wastewater using ZnO as semiconductor catalyst, *Journal of Hazardous Materials*, 112(3), 269-278.